Discovery Immunology, 2026, **5**, kyag022
https://doi.org/10.1093/discim/kyag022
Published: 11 November 2026
Research article

Pathogenesis and immune responses to Eurasian avian-like H1N1 and influenza D virus in pigs

Ashutosh Vats [1*], Liu Yang[1], Ehsan Sedaghat-Rostami [1,2], Catherine Hatton[1], Emily Briggs [1,2], Graham Freimanis [1], Tim Downing [1], Kristien van Reeth[3], Basudev Paudyal [1], Francisco J. Salguero[2,4], Wilhelm Gerner[1†] and Elma Tchilian[1*†]

[1]Host Responses, The Pirbright Institute, Pirbright, UK
[2]Faculty of Health and Medical Sciences, School of Biosciences, The University of Surrey, Guildford, UK
[3]Department of Translational Physiology, Infectiology and Public Health, Faculty of Veterinary Medicine, Ghent University, Ghent, Belgium
[4]United Kingdom Health Security Agency, UKHSA-Porton Down, Salisbury, UK
*Corresponding authors. Ashutosh Vats, Host Responses, The Pirbright Institute, Pirbright, UK. E-mail: ashutosh.vats@pirbright.ac.uk; Elma Tchilian, Host Responses, The Pirbright Institute, Pirbright, UK. E-mail: elma.tchilian@pirbright.ac.uk
†These authors share senior authorship.

Abstract

Introduction **Eurasian avian-like H1N1 (EAavH1N1) and influenza D viruses (IDV), with their ongoing evolution and zoonotic potential, are a serious threat to animal and human health. Using experimental infection of pigs, we characterized and compared their pathogenesis and immune responses.**

Methods **Pigs were infected intranasally with either IDV or EAavH1N1. We evaluated viral replication kinetics, respiratory tract pathology, local and systemic antibody and cellular immune responses, and conducted lung single-cell transcriptomics to assess changes at early and later infection stages.**

Results **EAavH1N1 induced rapid viral clearance and early immune activation, including robust systemic and mucosal antibody responses and increased IFNγ and TNF production. This heightened immune response was associated with more severe pathology of the upper and lower respiratory tract. In contrast, IDV infection resulted in prolonged viral shedding and higher viral titres, with delayed and attenuated cellular immune responses. Single-cell transcriptomic analysis of lungs further indicated early and persistent suppression of antiviral and innate immune pathways during IDV infection.**

Conclusion **These findings demonstrate that EAavH1N1 and IDV exhibit distinct viral kinetics, immune activation profiles, and lung responses, providing insight into differences in transmission dynamics, disease severity, and immune control among influenza virus types in swine.**

Keywords influenza D, Eurasian avian-like H1N1 virus, pig, scRNA seq, lung

Received: 21 May 2026. **Revised:** 19 August 2026. **Accepted:** 27 October 2026
© The Author(s) 2026. Published by Oxford University Press on behalf of the British Society of Immunology.
This is an Open Access article distributed under the terms of the Creative Commons Attribution License (https://creativecommons.org/licenses/by/4.0/), which permits unrestricted reuse, distribution, and reproduction in any medium, provided the original work is properly cited.

Graphical abstract

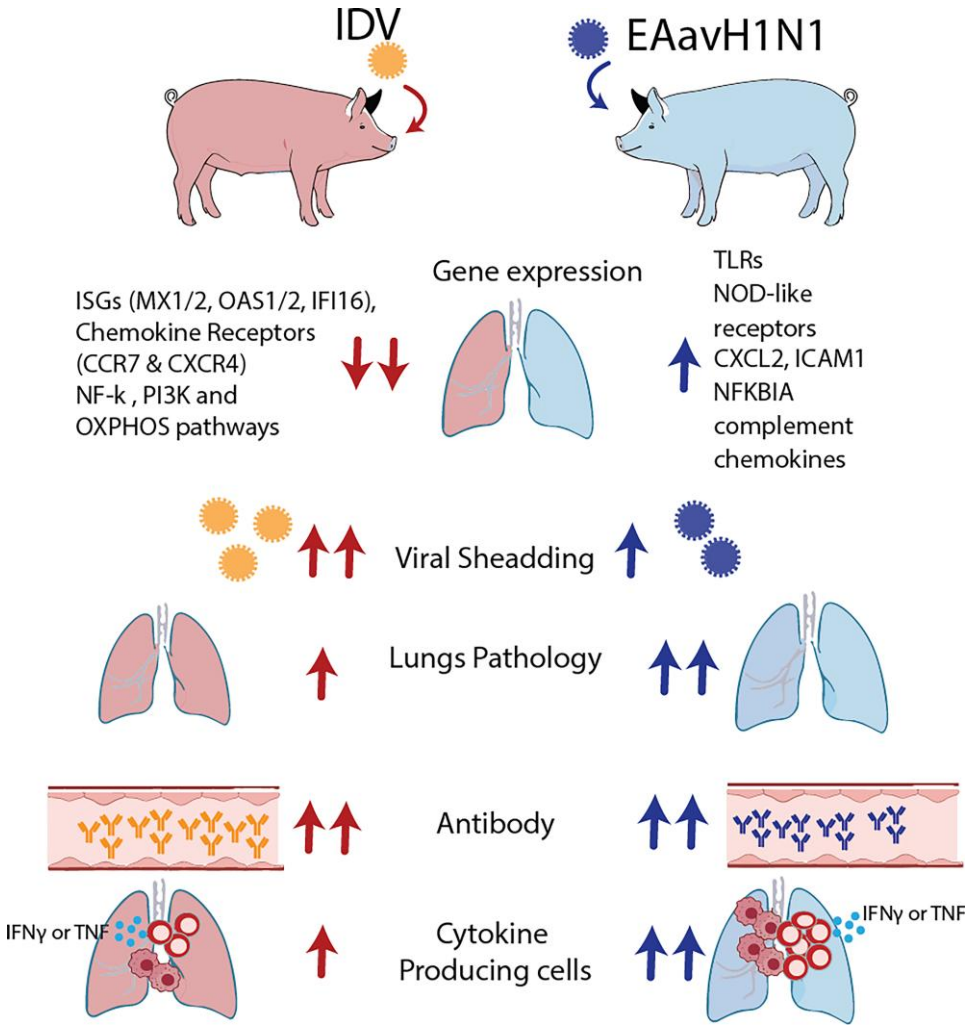

Introduction

Influenza viruses are a major threat to animal and human health, causing significant morbidity, mortality, and economic losses. Their ongoing antigenic and genomic evolution reduces the long-term effectiveness of vaccines and antiviral drugs [1]. Continued circulation and reassortment among humans, livestock, and wildlife drive the emergence of novel zoonotic variants with pandemic potential [2]. Pigs are a natural host and a potential mixing vessel at the human—livestock interface. Their respiratory tract expresses α2,3-linked and α2,6-linked sialic acid receptors, as well as 9-O-acetylated sialic acids, making them susceptible to avian-adapted and human-adapted influenza A viruses (IAV) and supporting infection by influenza D virus (IDV) [3, 4].

The Eurasian avian-like H1N1 (EAavH1N1) lineage remains a priority among swine IAVs due to its enzootic spread in Europe and Asia and its ability to reassort with other swine influenza viruses [5, 6]. Reassortment with internal genes from the 2009 pdmH1N1 and North American triple-reassortant swine viruses produced genotype 4 (G4) EAavH1N1 viruses that enable efficient replication in mammalian airways and greater affinity for human-type (α2,6-linked)receptors [7]. These features can facilitate cross-species transmission [7–9]. Surveillance continues to detect sporadic human infections with EAavH1N1-related viruses, including cases without direct pig contact, indicating that spillover can occur through unrecognized modes of transmission [8, 10, 11]. Experimental infection with EAavH1N1 indicates that it can cause respiratory disease in pigs ranging from moderate influenza-like illness with the G1 genotype to more severe lower respiratory tract pathology caused by the G4 genotype [12]. Similarly, studies in mice have shown that recent strains of the G4 EAavH1N1 lineage exhibit higher replication levels in lungs compared with earlier G1 viruses [13].

Influenza D virus has emerged more recently as an important pathogen at the livestock interface. In contrast to influenza A viruses, IDV has a seven-segment genome and a haemagglutinin esterase fusion glycoprotein, HEF, that combines receptor binding, receptor destroying and fusion functions [14–16]. HEF targets 9-*O*-acetylated sialic acids, which are abundant in cattle and present in pigs [6, 17]. IDV is actively diversifying, with multiple genetic and antigenic lineages circulating and evidence of reassortment [14]. Cattle are the main reservoir, but pigs are

susceptible, with serological and virological data indicating repeated exposure in domestic and wild swine populations [17–21]. Serological studies show high exposure among cattle- and swine-associated workers, even without sustained human-to-human spread [22–25]. Furthermore, recent studies demonstrated that IDV replicates efficiently in multiple human respiratory models while evading the innate immune defences, raising concerns that only minimal evolutionary changes may be required for sustained human transmission [26]. In cattle, IDV pathogenesis has been studied in much greater detail and is generally characterized by mild respiratory disease, efficient transmission and measurable airway innate responses, although some strains can also involve the lower respiratory tract and contribute to more severe disease in the context of coinfection with *Mycoplasma bovis* [21, 27, 28]. By contrast, in pigs, IDV infection has usually been described as subclinical or mild, with replication largely restricted to the upper respiratory tract [17–19]; however, recent evidence suggests that some strains may replicate efficiently and transmit between pigs [21, 29, 30].

Although both EAavH1N1 and IDV circulate in swine and are relevant to animal and public health, most studies have focused on virology, transmission, or serology, leaving limited understanding of the immune mechanisms that control infection or drive tissue damage. Importantly, these viruses exhibit contrasting infection profiles: EAavH1N1 causes acute infection involving both the upper and lower respiratory tract, whereas IDV generally produces largely subclinical infection associated with upper respiratory tract replication and shedding. Here, we used experimental infection with EAavH1N1 and IDV in pigs to define and directly compare their pathogenesis and immune control. We characterized viral replication kinetics, respiratory tract pathology, and local and systemic immune responses, together with lung transcriptomic changes across early and later stages of infection. By analysing these parameters side by side in the natural host, we identified lineage-specific differences in lung pathology and immune regulation, providing a more integrated understanding of influenza virus infection in swine.

Results

EAavH1N1 causes earlier lung pathology, whereas IDV shows prolonged replication

Fifteen pigs were infected intranasally either with D/swine/Netherlands/PS-497/2021 Influenza D virus (IDV) or A/swine/Gent/274/2020 (EAavH1N1). Six animals were left untreated as controls (Fig. 1a). At 1-, 5-, and 12-days post-infection (DPI), 5 animals per infected group and 2 controls were euthanized to assess early (1 and 5 DPI) and late events (12 DPI) following infection (Fig. 1a). Viral shedding was quantified by plaque assay and qRT–PCR of nasal swabs. Both viruses showed productive infection by 1 DPI, but IDV reached higher titres and persisted until 5 DPI, while EAavH1N1 shedding ended by 3 DPI (Fig. 1b, Supplementary Figure S1b, c and d). The nasal shedding of IDV was significantly higher than EAvH1N as analysed by the area under the curve $P = <0.0001$. No infectious virus or viral RNA was detected by 10 DPI.

Lung pathology was assessed by gross and histopathological scoring as previously described, including immunohistochemistry (IHC) for detection of viral nucleoprotein (NP) [31]. Lung pathology was variable between animals; however, the overall pattern was consistent: EAavH1N1 induced earlier and more severe pathology, detectable at 1 DPI, peaking at 5 DPI, with milder lesions still present at 12 DPI, while IDV showed milder lesions at 1 DPI, similar lesions at 5 DPI, and clearance at 12 DPI (Fig. 1c and Supplementary Figure S1a). Histopathological evaluation showed multifocal broncho-interstitial pneumonia after infection with either virus (Fig. 1d). Viral NP was observed within the airway epithelia and within the inflammatory cell infiltration in the alveoli luminae and interalveolar septa, at 1 and 5 DPI in EAavH1N1 and only at 5DPI in IDV-infected animals (Fig. 1e). EAavH1N1 induced significantly more severe pathology in the upper respiratory tract, particularly in the respiratory ($P = 0.048$) and olfactory ($P = 0.039$) turbinates, than IDV at 5 DPI (Fig. 1f).

Together, these data show that EAavH1N1 induced earlier and more severe pathology in the respiratory tract, while IDV resulted in higher and more prolonged nasal shedding.

Antibody responses to IDV and EAavH1N1

Virus-specific systemic and mucosal IgG and IgA responses were analysed in serum, bronchoalveolar lavage (BAL) and nasal swabs by ELISA and virus neutralization assays (Supplementary Figure S2). EAavH1N1-specific IgG in serum was detectable by 5 DPI and increased up to 12 DPI, whereas IDV-specific IgG appeared at 7 DPI and continued to increase up to 12 DPI (Supplementary Figure S2a). IgA titres followed a similar pattern to IgG although at lower titres. Virus-specific IgA appeared earlier after EAavH1N1 infection but was higher at 12 DPI in IDV-infected animals (Supplementary Figure S2d). In BAL, both IgG and IgA were detectable at 12 DPI in IDV-infected pigs and were higher compared to EAavH1N1 (Supplementary Figure S2b and e). BAL titres were low, reflecting the very diluted nature of sampling. Nasal swabs titres were also low, but detectable at higher levels in IDV samples at 10DPI (Supplementary Figure S2c and f). Serum neutralizing antibody activity mirrored the ELISA titres with higher levels in IDV than EAavH1N1 by 12 DPI (Supplementary Figure S2g). No neutralization was detected in the BAL and nasal swabs.

Taken together, these data indicate that EAavH1N1 induced earlier and stronger serum antibody responses than IDV. However, by 12 DPI virus-specific responses were higher in IDV-infected animals in serum, BAL, and nasal swabs compared to EAavH1N1. Although endpoint titres provide a relative measure that reduces the influence of differences in absolute optical density between antigen preparations, direct quantitative comparisons between different antigens should be interpreted with caution because of potential differences in antigen coating efficiency, epitope density, and epitope presentation.

Cytokine responses following EAavH1N1 and IDV infection

Virus-specific cytokine-secreting cells were quantified in BAL, tracheobronchial lymph nodes (TBLN), peripheral blood mononuclear cells (PBMC), and spleen using ELISpot IFNγ and IL-2

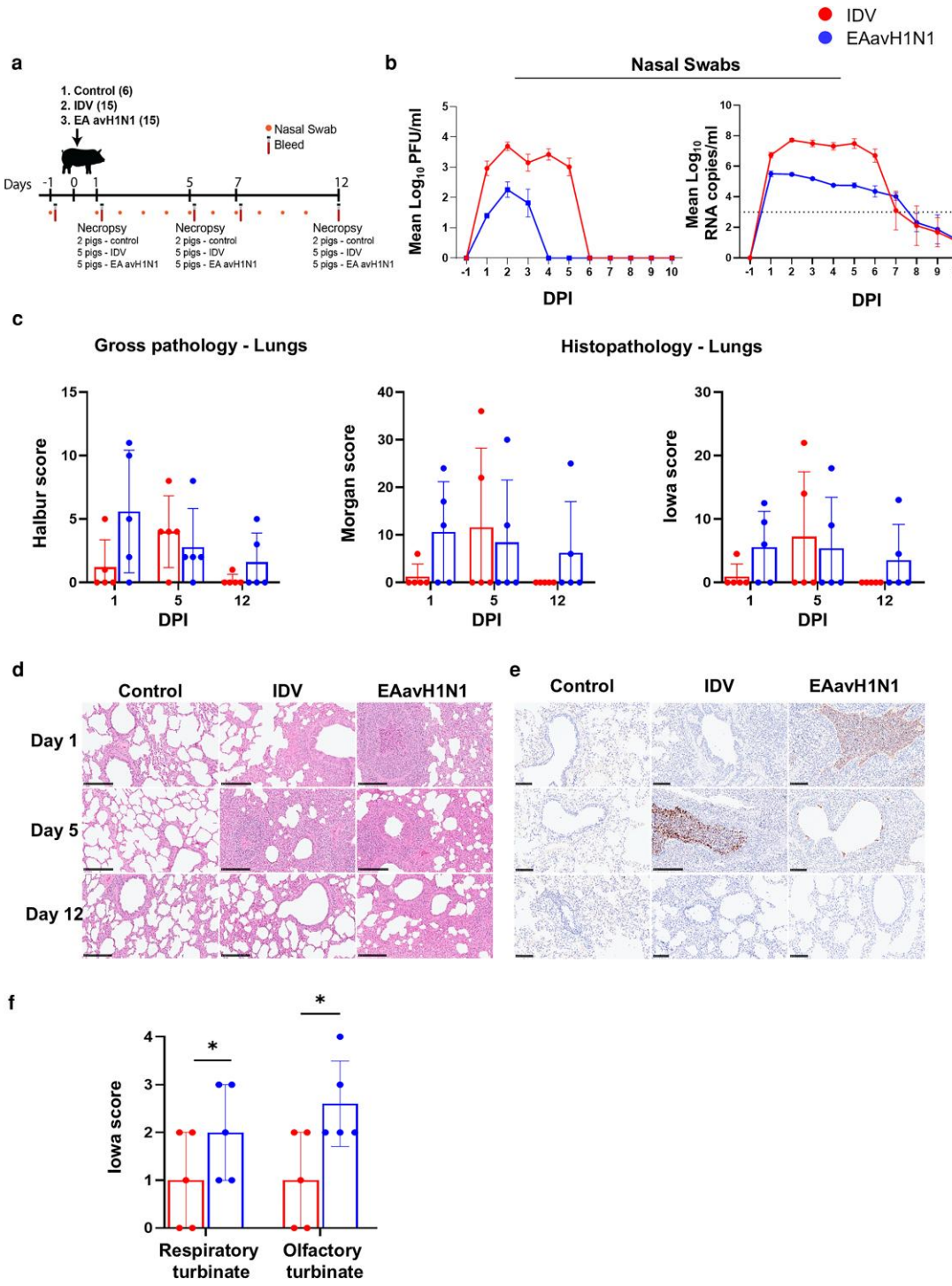

Figure 1 Experiment design, lung pathology and viral shedding post IDV and EAavH1N1 infection. (a) Thirty-six pigs were divided into three groups: untreated controls ($n = 6$), avH1N1-infected ($n = 15$), and IDV-infected ($n = 15$). Daily nasal swabs were taken through day 10 to monitor viral shedding. Necropsies were performed on Days 1, 5, and 12, with 2 control, 5 avH1N1, and 5 IDV pigs per timepoint for lung pathology. (b) Viral titres were measured by plaque assay and RT-qPCR. Swab samples were collected from day −1 to day 10 post-infection for both IDV and EAavH1N1 groups. Results are shown as mean Log_{10} *PFU*/ml or Log_{10} RNA copies/ml. Data are presented as mean ± SEM, with each dot representing the mean value. Lung sections from each group were assessed for gross pathology, histopathology (H&E staining), and viral nucleoprotein (NP) distribution by IHC. (c) Gross pathology, and histopathology (Morgan and Iowa). (d) Histopathology revealed bronchiolo-interstitial pneumonia with epithelial necrosis and inflammatory infiltrates. (e) NP-IHC staining observed mainly in the bronchiolar epithelial cells and inflammatory cell infiltrates and exudates (brown staining) (f). Histopathology and immunohistochemistry scores of the respiratory ($P = 0.048$) and olfactory ($P = 0.039$) turbinate in IDV, and EAavH1N1 at 5 DPI. In (c) and (f), data are shown as mean ± SD, with each dot representing an individual animal. In (f), asterisks indicate significance between groups (*$P < 0.05$). Data were analyzed using two-way ANOVA followed by Bonferroni's multiple-comparisons test for normally distributed data. Scale bar = 100 μm, SD = standard deviation, SEM = standard error of the mean.

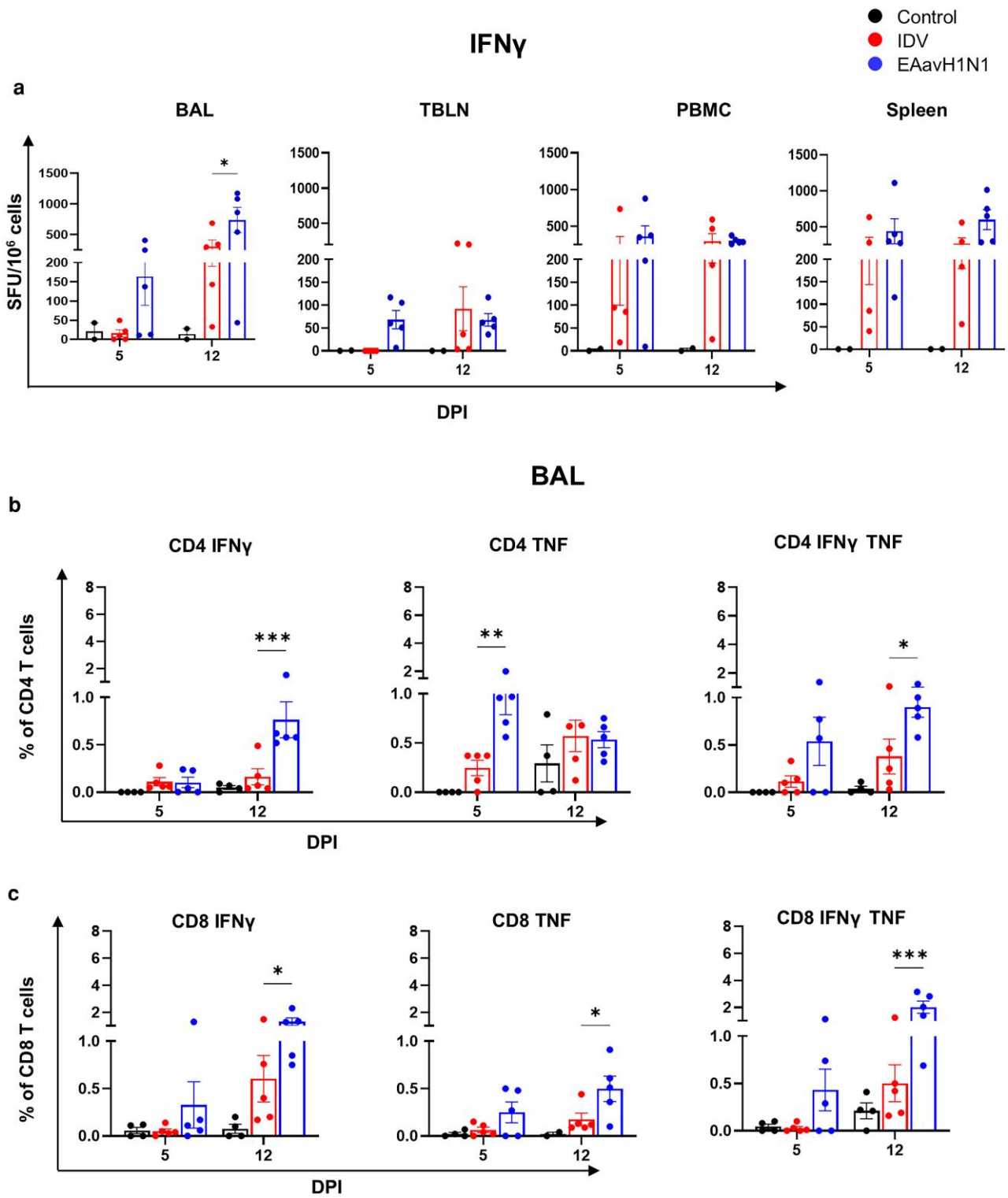

Figure 2 Virus-specific T-cell responses by ELISpot and intracellular cytokine staining (ICS). (a) Cells producing IFNγ in BAL, TBLN, PBMC, and spleen in response to whole live IDV or EAavH1N1 virus at the indicated timepoints were measured by ELISpot. Symbols in A represent mean spot-forming units (SFU) per group, with error bars indicating. (b, c) IFNγ- and TNF-producing $CD4^+$ and $CD8^+$ T cells were measured by intracellular cytokine staining following stimulation with whole virus at the indicated timepoints. Data are presented as mean ± SEM, with symbols indicating individual animals. Normally distributed data (a–c) were analysed by two-way ANOVA followed by Bonferroni's multiple comparisons test. Asterisks denote statistically significant differences between IDV and EAavH1N1 responses at indicated timepoint time points (**$P < 0.05$, ***$P < 0.01$, ****$P < 0.001$).

assays after *ex vivo* stimulation with live IDV or EAavH1N1 viruses (Fig. 2a and Supplementary Figure S3). EAavH1N1 induced IFNγ ELISpot-secreting cells in BAL and TBLN by 5 DPI, which increased by 12 DPI and were significantly higher compared to IDV in BAL. In PBMC and spleen, IFNγ ELISpot responses were comparable between IDV and EAavH1N1 at 5 and 12 DPI

(Fig. 2a). Interleukin 2 responses showed similar kinetics to IFNγ but were lower overall (Supplementary Figure S3).

Intracellular cytokine staining (ICS) was performed to identify the responding IFNγ$^+$ and TNF CD4$^+$, CD8$^+$, and γδ$^+$ T cell subsets (Fig. 2b, c and Supplementary Figures S4, S5, S6, S7). In BAL, EAavH1N1 infection significantly increased the proportions of IFNγ$^+$ and TNF$^+$ CD4$^+$ cells at 12 DPI compared to IDV and of IFNγ$^+$TNF$^+$ CD4$^+$ T cells at 5DPI (Fig. 2b). CD8$^+$ T cells exhibited a similar pattern, with significantly higher frequencies of IFNγ$^+$, TNF$^+$, and IFNγ$^+$TNF$^+$ CD8$^+$ cells at 12 DPI in EAavH1N1-infected animals compared to IDV (Fig. 2c).

PBMC and spleen responses also showed significantly higher proportions of cytokine-secreting CD4$^+$ and CD8$^+$ cells in EAavH1N1-infected animals (Supplementary Figure S5a, b). Responses in TBLN were low, but still higher for both CD4 and CD8 cytokine-producing cells in EAavH1N1-infected animals (Supplementary Figure S6). γδ T cell cytokine responses were low overall, but were higher in EAavH1N1-infected pigs, especially in BAL and TBLN, except that IFNγ$^+$TNF$^+$ γδ$^+$ T cells in IDV-infected pigs in TBLN (Supplementary Figure S7).

Overall, these data indicate that both viruses induced virus-specific cytokine production in T cells following *in vitro* restimulation infection, with a higher proportion of IFNγ and TNF-secreting cells observed in EA avH1N1-infected animals compared to IDV.

Differential abundance analysis reveals infection-specific cellular response in the porcine lung

Single-cell (sc) RNA-seq was performed from lung tissue-derived cell suspensions of control pigs ($n = 3$), IDV-infected pigs ($n = 3$ at 1 DPI; $n = 4$ at 12 DPI), and EAavH1N1-infected pigs ($n = 4$ at 12 DPI), resulting in 14 samples. All five 1DPI EAavH1N1 samples showed reduced cell viability and were therefore excluded from the scRNA-seq analysis. Although a technical contribution cannot be ruled out, the lower viability may partly reflect the more severe early lung inflammation and tissue damage induced by EAavH1N1. After unsupervised clustering, we identified three main compartments: myeloid, lymphoid, and non-immune cells with multiple cell subpopulations in each compartment (Supplementary Figure S8a–d). Infection status significantly influenced the composition of these three major cellular compartments, accounting for 48% of the total variance (PERMANOVA: $F = 3.09$, $r^2 = 0.48$, $P = 0.022$). Their proportions suggested potentially more myeloid cells in IDV-infected pigs at 1 DPI, and possibly more lymphoid ones at 12 DPI for both infections (Supplementary Figure S8e).

Reduced expression of immune genes and metabolic pathways in lung cell populations during IDV infection

Differential gene expression for IDV samples from 1 DPI compared to control samples showed reduced expression of genes across several cell types present within myeloid, lymphoid and non-immune cells (Fig. 3). Myeloid cells (Fig. 3a, Supplementary Table S1) showed a modest but consistent reduced expression of genes linked to basic cellular functions, including pyrimidine metabolism (DPYS), stress–response chaperones (HSPA6), and lysosome-related vesicle trafficking (HPS5), suggesting reduced metabolic and stress-response activity (Fig. 3b, Supplementary Table S2). In lymphoid populations (Fig. 3c, Supplementary Table S2), a broader set of antiviral and interferon-associated genes (including DDX60, EIF2AK2, MX1, and RSAD2) was lower in IDV-infected pigs, indicating a low antiviral response in early infection. A similar pattern was observed in non-immune cells, particularly in endothelial-like populations, which exhibited widespread reduced expression of interferon-stimulated and viral sensing genes involved in innate immune defence (e.g. ZBP1, IFIT1, IFIT2, IFIT3, DDX60, EIF2AK2, USP18, CMPK2, MX1, MX2, IFI44, IFI44L, IRF7, OAS1, OAS2, IFIH1, HERC5, HERC6, DHX58, RIGI/DDX58, ADAR, PLSCR1, PML and PARP9/PARP12/PARP14) (Fig. 3d, Supplementary Table S3). This was also reflected in the gene set enrichment analysis (GSEA), where across the three compartments at least one cell population showed altered NOD-like receptor, RIG-I-like receptor and Toll-like receptor signalling or cytosolic DNA sensing (Fig. 3e, Supplementary Table S4). Overall, these findings suggest a coordinated suppression of antiviral and stress-response pathways across multiple lung cell compartments at this early stage of IDV infection.

At 12 days post-infection, some cell clusters across the three major cell compartments showed increased gene expression compared to control pigs, but reduced gene expression still dominated (Fig. 4a). Several myeloid cell clusters displayed a consistent downregulation of genes involved in transcriptional regulation (CEBPB) and core components of the translational machinery (RPL38, RPS29, SEC61G) (Fig. 4b, Supplementary Table S1), indicating reduced protein synthesis and altered cellular activity. In lymphoid populations, a large set of shared DEGs across T, B, and NK cells was dominated by genes with reduced expression that are linked to mitochondrial respiration (ATP5ME, ATP5MK, COX17, COX6C, NDUFB1), ribosomal function (RPL37, RPL37A, RPL38, RPS25, RPS26, RPS28, RPS29), and immune signalling (CEBPB, JUNB, MAP2K3, ZFP36L2) (Fig. 4c, Supplementary Table S2). This pattern suggests a broadly suppressed transcriptional and metabolic state across lymphoid lineages. Non-immune cells showed a similar trend (Fig. 4a), with reduced transcriptional expression of ribosomal (RPL38, RPS29, RPS28, RPL37, and RPL37A), protein-processing (SEC61G), and post-transcriptional regulatory genes (ZFP36L2) (Fig. 4d, Supplementary Table S3). GSEA analysis showed similar pathways were affected as at 1DPI (e.g. NOD-like receptor signalling, Toll-like receptor signalling, cytosolic DNA sensing) across several cell clusters in the three cell compartments (Fig. 4e, Supplementary Tables S4, S5) and additional chemokine signalling and antigen processing/presentation. Overall, these findings point to a coordinated shift towards reduced protein synthesis and immune activity, combined with altered mitochondrial function, across multiple lung cell compartments at this later stage of infection.

At 12DPI EA avian H1N1 infection is characterized by a recovery-associated gene pattern

Compared to IDV, the number of differentially expressed genes (DEGs) for EAavH1N1-infected pigs in relation to controls at 12 DPI was considerably lower across all three cell compartments

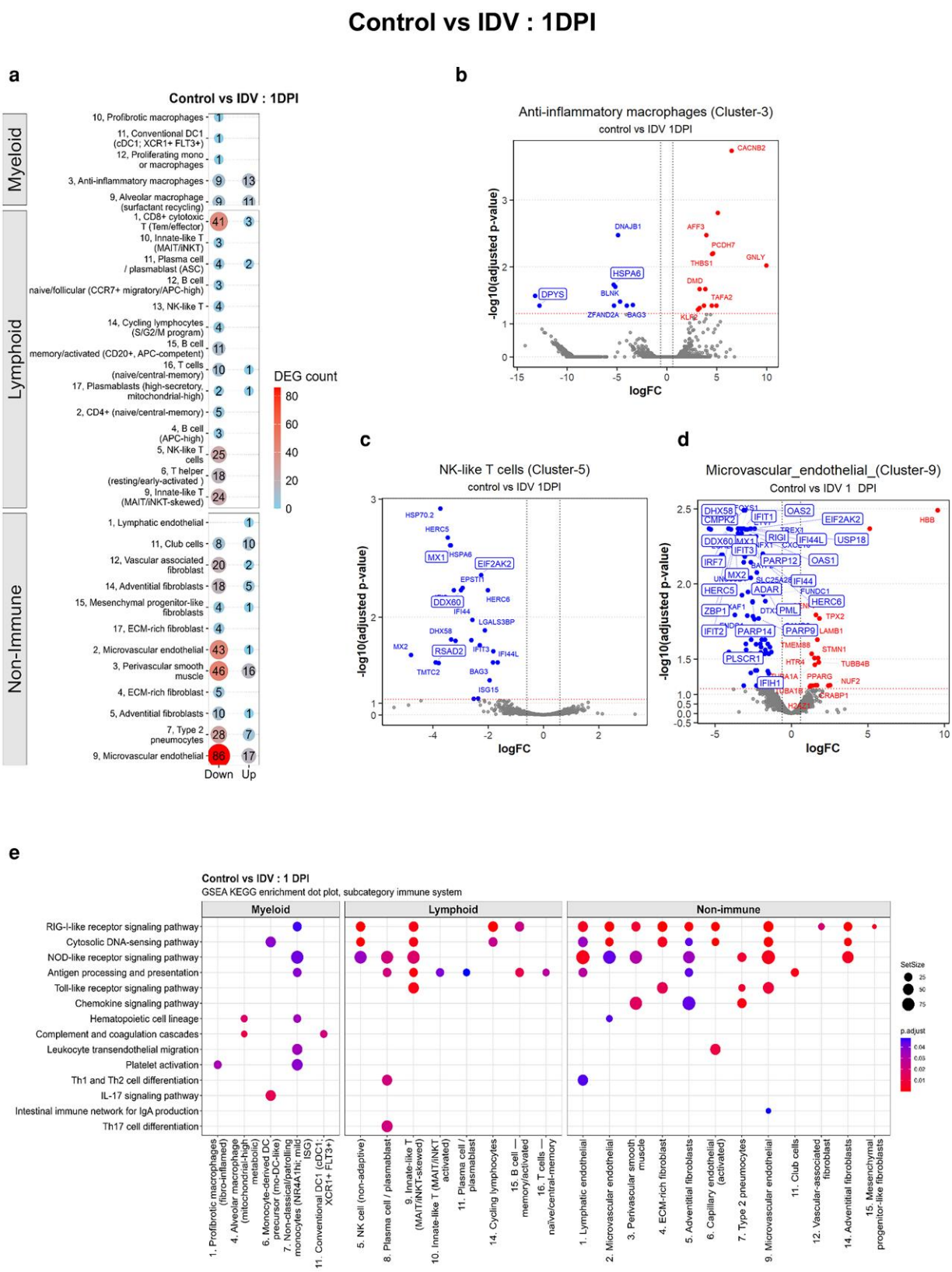

Figure 3 Myeloid, lymphoid, and non-immune cell programs show distinct responses during early IDV (1DPI) infection in pig lung. (a) Bubble heatmap shows the number of differentially expressed genes (DEGs) per subset compared to the control. Numbers preceding each cell type indicate the cluster number within each cell compartment. (b, c) Volcano plot displays a representative cell subtype, with each point representing a gene coloured by expression direction (red: upregulated; blue: downregulated; grey: not significant), plotted by log fold change (logFC) versus −log10 adjusted *P* value. (e) Dot plot shows KEGG GSEA results for the same cell compartment, where dot size indicates set size and dot colour reflects adjusted enrichment significance (p.adjust).

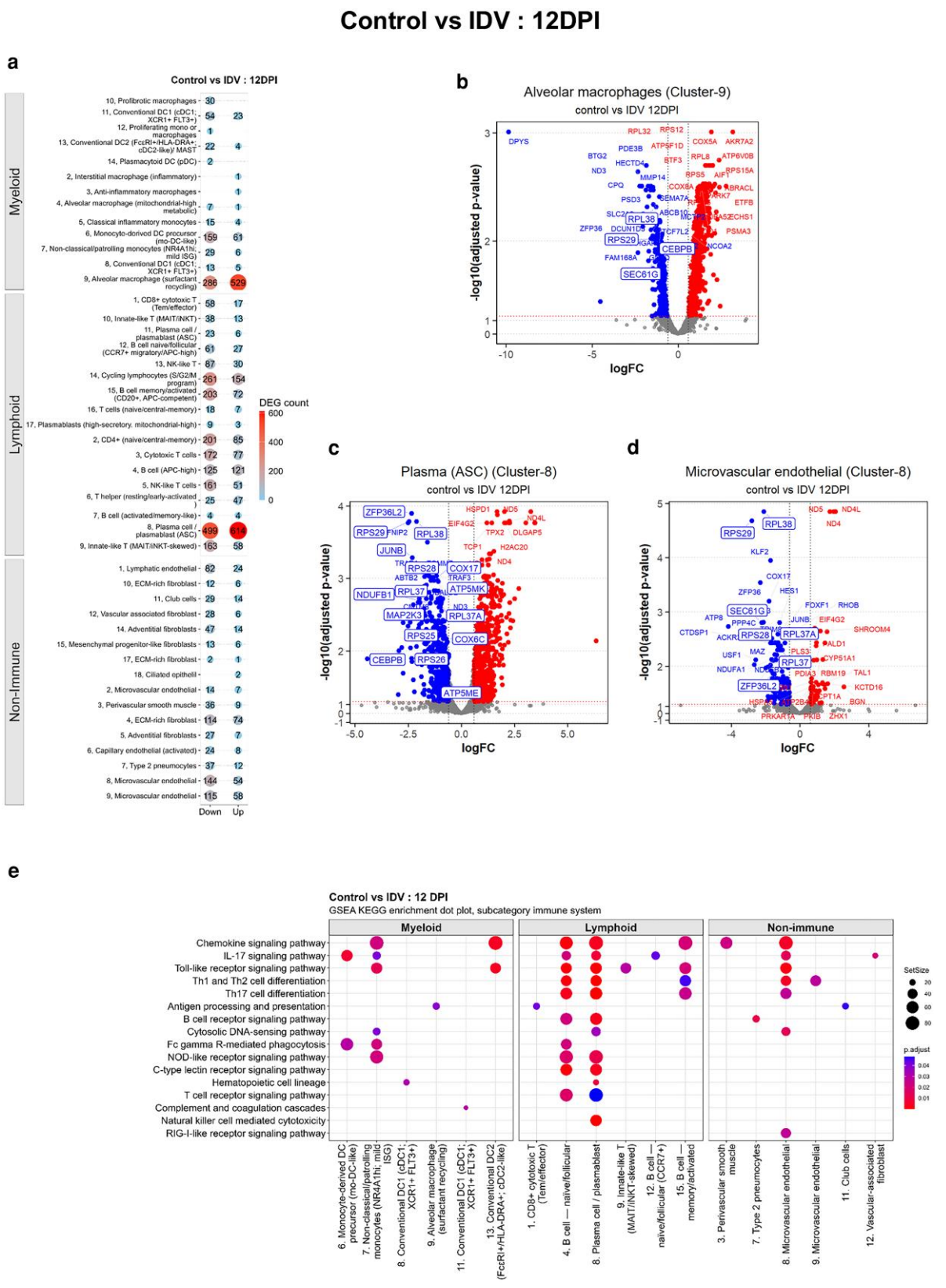

Figure 4 Myeloid, lymphoid, and non-immune cell programs show distinct responses during late IDV (12DPI) infection in pig lung. (a) Bubble heatmap shows the number of differentially expressed genes (DEGs) per subset in IDV infection group compared to the control. Numbers preceding each cell type indicate the cluster number within each cell compartment. (b, c) Volcano plot displays a representative cell subtype, with each point representing a gene coloured by expression direction (red: upregulated; blue: downregulated; grey: not significant), plotted by log fold change (logFC) versus −log10 adjusted *P* value. (e) Dot plot shows KEGG GSEA results for the same cell compartment, where dot size indicates set size and dot colour reflects adjusted enrichment significance (p.adjust).

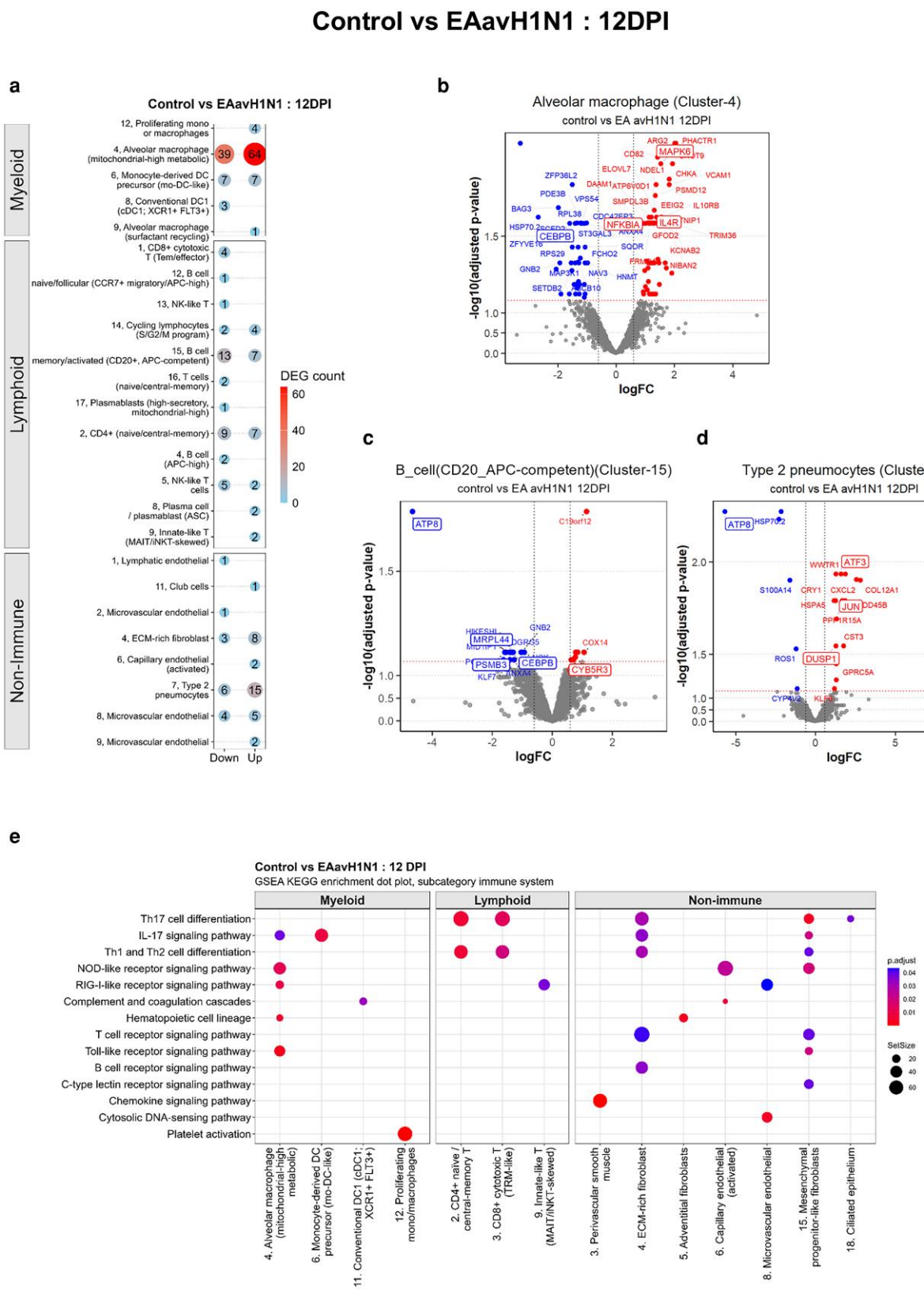

Figure 5 Myeloid, lymphoid, and non-immune cell responses during late EAavH1N1 (12DPI) infection in pig lung. (a) Bubble heatmap shows the number of differentially expressed genes (DEGs) per subset in EA avH1N1 infection group compared to the control. Numbers preceding each cell type indicate the cluster number within each cell compartment. (b, c) Volcano plot displays a representative cell subtype, with each point representing a gene coloured by expression direction (red: upregulated; blue: downregulated; grey: not significant), plotted by log fold change (logFC) versus −log10 adjusted *P* value. (e) Dot plot shows KEGG GSEA results for the same cell compartment, where dot size indicates set size and dot colour reflects adjusted enrichment significance (p.adjust).

(Fig. 5a). In myeloid cells, differential expression was primarily found in alveolar macrophage cluster 4, which showed an increased expression of NF-κB inhibitory and signalling modulators (NFKBIA, IL4R, MAPK6) alongside reduced expression of the pro-inflammatory transcription factor CEBPB (Fig. 5b, Supplementary Table S1). In lymphoid populations, a reduced expression of genes involved in protein synthesis, metabolism, and immune signalling (MRPL44, PSMB3, ATP8, CEBPB) was found across T, B, and NK cell lineages, with only limited upregulation of genes linked to metabolic or chromatin-related functions (CYB5R3, H2AC20) (Fig. 5c, Supplementary Table S2). Non-immune cells displayed a partially overlapping pattern, with reduced expression of metabolic and housekeeping genes (ATP8, SEC61G) alongside induction of stress- and signalling-related genes (JUN, ATF3, DUSP1) (Fig. 5d, Supplementary Table S3), indicating tissue adaptation rather than active inflammation. While transcriptional data from EAavH1N1-infected pigs at 1 DPI could not be analysed, these findings suggest a transition from early antiviral responses to a more recovery- or resolution-associated state across lung cell compartments. This is also reflected in the GSEA results that show an alteration of signalling pathways present in different cell types, ranging from innate immune cells to platelets and adaptive immune cells (Fig. 5e, Supplementary Tables S4, S5).

Differential metabolic and translational gene expression distinguishes IDV from EAavH1N1

Finally, we compared scRNA-seq data from 12 DPI from the two viral infections against each other, with EAavH1N1 as the baseline. The total number of DEGs was high across all the major cell types (Fig. 6a). In myeloid cells, the strongest changes were observed in interstitial macrophages, monocyte-derived DC precursors, and dendritic cell populations, showing increased expression of ribosomal and metabolic genes (e.g. RPS28, RPS29, ATP5ME, COX17) and reduced expression of mitochondrial-encoded genes (e.g. ND4, ND5) (Fig. 6b, Supplementary Table S1). A similar pattern was found in lymphoid populations, where the highest DEG numbers were found in clusters representing plasmablasts, B cells, and $CD8^+$ and $CD4^+$ T-cell subsets, again characterised by increased expression of ribosomal and metabolic genes (e.g. RPS28, RPS29, ATP5ME) and reduced mitochondrial gene expression, with additional modulation of regulatory genes such as HES1 (Fig. 6c, Supplementary Table S2).

In non-immune cells, this pattern was most prominent in microvascular endothelial (cluster 8) and lymphatic endothelial cells (cluster 1), followed by fibroblast and perivascular populations, with increased expression of biosynthetic and signalling-associated genes (e.g. JUN, ATF3, CCL14) and reduced expression of mitochondrial and housekeeping genes (ND4, ND4L, ND5) (Fig. 6d, Supplementary Table S3). This was also reflected in GSEA analyses, which showed that multiple signalling pathways present in innate and adaptive immune cells, but also in other cell types, were altered (Fig. 6e, Supplementary Tables S4, S5). Overall, these findings indicate changes in cellular metabolism and protein synthesis across immune and structural cell types, distinguishing the IDV response strongly from EAavH1N1 at 12DPI.

Discussion

The present study provides a comparative analysis of host responses to two antigenically and biologically distinct swine influenza viruses, showing clear differences in infection kinetics, respiratory pathology, and immune responses. The data indicate early, robust host responses associated with EAavH1N1 and a more prolonged, yet immunologically attenuated, profile following IDV infection.

IDV shedding persisted longer with higher titres, suggesting either more efficient replication or delayed clearance at mucosal surfaces. In contrast, EAavH1N1 triggered rapid tissue damage in both upper and lower respiratory tract compartments, indicating that early host responses contribute to pathology. These findings are broadly consistent with previous work in pigs and other animal models. Experimental infections with EAavH1N1 in swine show efficient replication in both the upper and lower respiratory tract and the development of cranioventral bronchopneumonia [32, 33]. Studies of reassortant EAavH1N1 viruses in mice have further demonstrated that specific gene constellations, particularly those incorporating pandemic 2009 internal genes or polymerase mutations, significantly increase replication and inflammatory responses, leading to more severe lung pathology [9, 12, 34]. Ferret models have shown efficient replication and transmission with only moderate pathology, suggesting that host species and viral genotype together determine disease severity [35].

In contrast, the more prolonged but clinically attenuated profile for IDV observed here is in agreement with reports from cattle, where infection is typically mild, often restricted to the upper respiratory tract, and associated with efficient transmission but limited overt pathology unless compounded by coinfection [21, 27, 28]. Similarly, in guinea pigs and ferrets, IDV has been shown to reach substantial viral loads in the respiratory tract, in some cases including the lower respiratory tract, yet with minimal clinical signs [36, 37]. The contrasting infection profiles of these two naturally circulating swine viruses also provide insight into the importance of the upper respiratory tract in determining infection outcome. IDV maintained substantial and prolonged upper respiratory tract replication and shedding despite limited clinical disease, whereas EAavH1N1 induced stronger inflammatory responses and more extensive respiratory pathology but was cleared more rapidly. These findings indicate that efficient replication and shedding from the upper respiratory tract do not necessarily predict disease severity and suggest that the anatomical distribution of infection and the nature of the local host response are important determinants of the balance between viral transmission, pathology and clearance.

The differences between IDV and EAavH1N1 are also reflected in the antibody responses. EAavH1N1 elicited earlier systemic IgG and IgA responses, as well as earlier neutralizing activity, consistent with faster antigen presentation and immune priming. In contrast, IDV induced a delayed but ultimately higher antibody response in serum, BAL, and nasal swabs at 12 DPI. This likely reflects prolonged antigen exposure due to sustained viral replication. The absence of detectable neutralizing activity in mucosal samples, despite measurable IgA, suggests that local antibodies

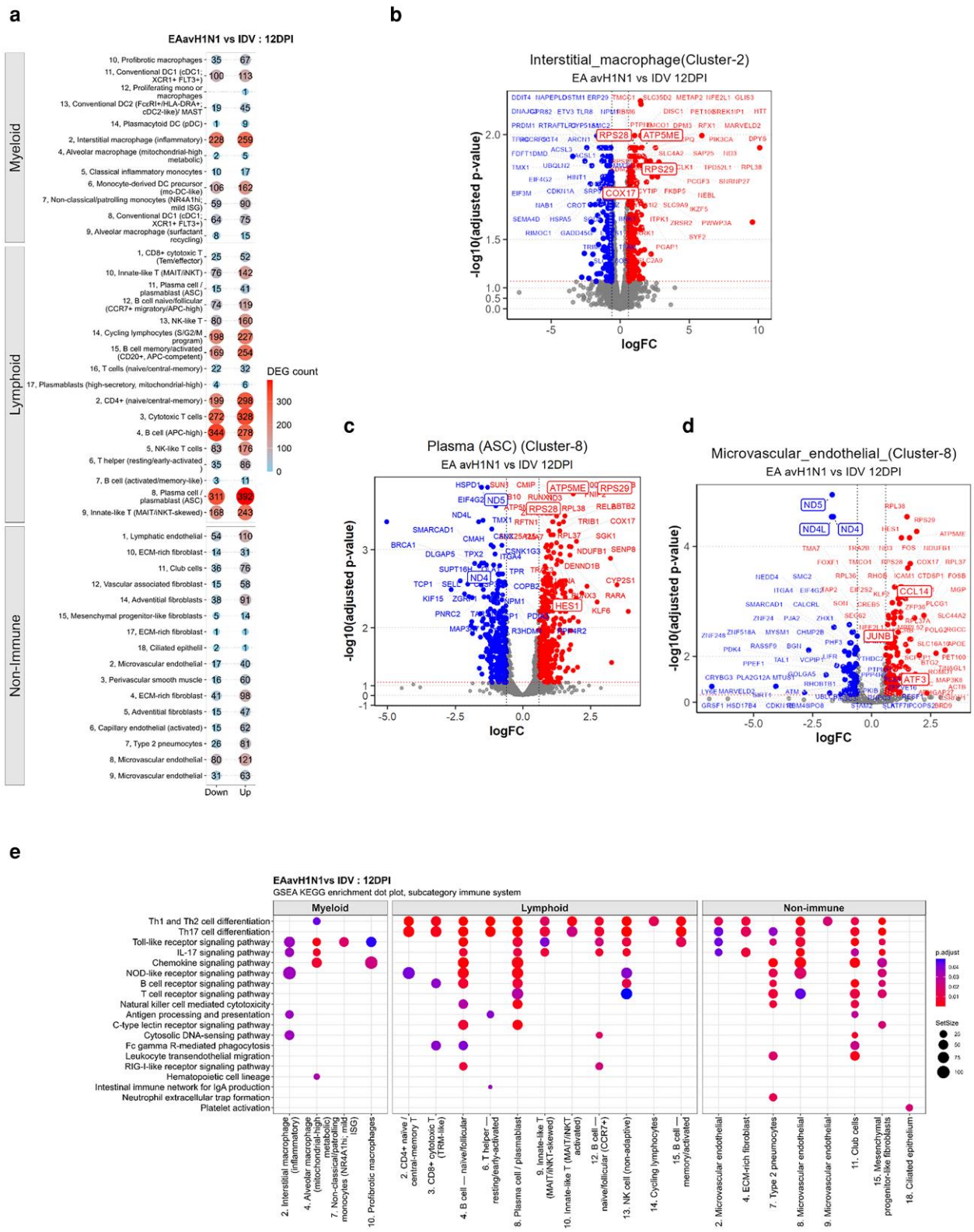

Figure 6 EAavH1N1 and IDV elicit distinct transcriptional and pathway responses in lung cell compartments at 12 DPI. (a) Bubble heatmap shows the number of differentially expressed genes (DEGs) per subset in IDV infection group compared to the EAavH1N1. Numbers preceding each cell type indicate the cluster number within each cell compartment. (b, c) Volcano plot displays a representative cell subtype, with each point representing a gene coloured by expression direction (red: upregulated; blue: downregulated; grey: not significant) in IDV infected group, plotted by log fold change (logFC) versus −log10 adjusted *P* value. (e) Dot plot shows KEGG GSEA results for the same cell compartment, where dot size indicates set size and dot colour reflects adjusted enrichment significance (p.adjust).

may be non-neutralizing, below detection thresholds because of the diluted nature of the samples.

The two infections were further distinguished by their cellular immune responses. EAavH1N1 induced higher numbers of IFNγ and TNF-producing cells in BAL and TBLN, with responses also detected in PBMC and spleen, indicating a stronger activation of adaptive immunity. In contrast, IDV elicited weaker cytokine responses despite prolonged viral presence. The strong IFNγ and TNF responses induced by EAavH1N1 in this study are consistent with observations in more pathogenic influenza A infections, including murine models of reassortant EAavH1N1 where elevated IL-6, TNF, IFNγ and chemokine responses correlate with increased lung pathology [9, 12].

Single-cell transcriptomic analysis provided mechanistic insights into these observations. As early as 1 day post-infection, IDV infection was associated with widespread downregulation of interferon-stimulated genes and antiviral pathways across myeloid, lymphoid, and structural cell populations. Key components of viral sensing and innate immune activation, including RIG I-like receptor and Toll-like receptor signalling pathways, were reduced. While correlative, these findings suggest that IDV can reduce early innate immune responses, which may contribute to higher viral load and prolonged shedding. At the same time, this reduced antiviral signalling may limit inflammation and contribute to the milder lung pathology observed in IDV-infected pigs. The early downregulation of interferon-stimulated genes and innate sensing pathways during IDV infection is consistent with experimental evidence in cattle indicating limited type I interferon activation and with the known role of viral proteins in suppressing host responses [27, 29, 38].

This low transcriptional activity by IDV persisted at 12 DPI, extending to genes involved in protein synthesis, mitochondrial function, and immune signalling across all major lung cell compartments. Such coordinated downregulation indicates a sustained alteration of lung tissue homeostasis and may explain the reduced local T cell responses in BAL, potentially reflecting a microenvironment less supportive of type 1 T cell response. Despite this, IDV-infected pigs showed higher antibody titers in serum and BAL. One possible explanation is that prolonged viral replication enhances antigen delivery to draining lymph nodes; this may have supported B cell activation and antibody production, even if local lung responses were low.

In contrast, EAavH1N1 infection at 12 DPI showed fewer transcriptional changes relative to controls, with gene expression patterns consistent with resolution and tissue repair. Reduced expression of pro-inflammatory and metabolic genes, alongside induction of regulatory and stress response pathways, suggests that viral clearance had occurred and that lung tissue was transitioning towards recovery.

Several limitations of this study should be acknowledged. First, each virus was represented by a single isolate, and strain-specific variation, particularly within the EAavH1N1 lineage, may limit the generalizability of our findings. Second, the experimental challenge dose was higher than during natural exposure to ensure consistent and synchronized infection at defined sampling points. Lung lesion scores also showed within-group variation. Viral load was quantified only in nasal swabs, limiting assessment of virus replication in different respiratory compartments, while interferon responses were assessed at the transcriptional rather than protein level. Finally, the absence of high-quality day 1 EAavH1N1 single-cell RNA sequencing data limited direct comparison of the earliest transcriptional responses to the two viruses. Future studies with multiple viral isolates, transmission models, compartment-specific viral quantification, and early local immune response will be important to validate and extend our results.

Overall, these findings support a model in which EAavH1N1 induces rapid and strong immune activation that drives early respiratory pathology but enables efficient viral clearance and recovery. In contrast, IDV causes a more prolonged infection characterized by higher viral replication, delayed and weaker immune responses, and sustained suppression of antiviral and metabolic pathways. These differences have important implications for transmission dynamics, disease outcome, and immune control of influenza viruses in swine and are also relevant for human health in settings with frequent pig-human interactions, such as in pig farming. By combining virological, pathological, cellular, and transcriptional analyses, this study provides a comprehensive benchmark against which the pathogenicity and host responses induced by other respiratory viruses can be compared. These data also establish a well-characterized porcine model that can be used to evaluate novel vaccine strategies, antiviral therapies and other interventions.

Materials and methods

Viruses

This study used IDV (D/swine/Netherlands/PS-497/2021, GenBank accession numbers OP474071–OP474077) and EAavH1N1 (A/swine/Gent/274/2020, GenBank accession numbers OP458671–OP458678) [6]. Both viruses were propagated and quantified in Madin-Darby Canine Kidney (MDCK) cells. Viral titers were determined by plaque assay and reported as plaque-forming units per millilitre (*PFU*/ml).

IDV and EAavH1N1 infection

Animals were acclimatized for at least 7 days and randomized into different groups and pens using Excel by the animal services staff. Researchers processing the samples were only aware of the pig numbers, not the group assignments. The pathologists were blinded to the group allocation when assessing the samples for gross pathology during *post-mortem* examination and subsequently during the histopathological assessment. All conditions were identical between the groups.

For infection studies, 36 five-week-old female 50% Landrace × 50% White Durocs cross (PIC Camborough 50) pigs (9–13 kg; mean 11.8 kg) were sourced from Home—PIC UK high-health commercial herd. All animals were seronegative for influenza A and D virus antibodies by ELISA with H1N1pdm09, IDV, and EAavH1N1. Pigs were randomly assigned to three groups: IDV-infected ($n = 15$), EAavH1N1-infected ($n = 15$) and untreated controls ($n = 6$). Pigs were intranasally infected with 6×10^6 *PFU*/ml of either IDV or EAavH1N1 or DMEM w/o antibiotics, 1.5 ml per nostril, using a mucosal atomization device (MAD; Wolfe-Tory Medical) following sedation following sedation with a 3 mg/kg Zoletil and 1.5 mg/kg Stresnil. Clinical parameters including demeanour, appetite, respiratory signs, sneezing, coughing, nasal and eye discharge, faeces consistency, and rectal

temperature were assessed. No significant clinical signs were observed in any of the pigs following the viral inoculation.

Nasal swabs were collected daily for 10 days post-infection (DPI) to assess viral load by plaque assay and RT-qPCR. Pigs were humanely euthanized with intravenous pentobarbital (Dolethal, 200 mg/ml) on days 1, 5, and 12 DPI, along with uninfected controls. At post-mortem, serum, PBMCs, lungs, tracheobronchial lymph nodes (TBLN), spleen, and bronchoalveolar lavage (BAL) were collected for analysis of viral load, pathology, immune responses, and scRNA-seq analysis.

Lung gross pathology, histopathology, and immunohistochemistry

Gross and histopathological analyses were performed as previously described [39]. Lungs were removed, and dorsal and ventral aspects were evaluated and digital images acquired to quantify the surface area showing pneumonia using image analysis software (Nikon NIS-Ar). Samples from the cranial, middle, and caudal lobes of the right lung were collected into 10% neutral-buffered formalin, paraffin-embedded, sectioned at 4 μm, and stained with haematoxylin and eosin (H&E). Immunohistochemistry (IHC) for IDV and EAavH1N1 viruses' nucleoprotein (NP) was performed on parallel sections [39, 40]. Histopathological changes were evaluated by a veterinary pathologist blinded to treatment groups. Lung histopathology was scored across five parameters: bronchiolar epithelial necrosis, airway inflammation, perivascular/bronchiolar cuffing, alveolar exudates, and septal inflammation on a 0–4 scale, yielding a maximum of 20 per lobe ($\sim 1.5 \times 3 \times 1.5$ cm^2) and 60 per animal. A cumulative score from the three lobes was calculated for each animal. Viral antigen distribution was additionally evaluated using the 'Iowa' scoring system. IHC labelling was assessed separately in bronchioles and alveoli, with each scored 0–3 [41]. The same scoring system was used to evaluate lesions and the presence of viral NP in the respiratory and olfactory nasal epithelium.

Sample processing and cell isolation

Serum, nasal swabs, PBMCs, and BAL were collected and processed as previously described [39, 42]. Mononuclear cells were isolated from lungs, TBLN, and spleens. TBLNs were minced, filtered through 70- and 40-μm strainers, washed, and resuspended in complete RPMI with 2% fetal bovine serum (FBS) and 1× Penicillin-Streptomycin (PS) [42]. Spleens were mechanically dissociated, filtered, centrifuged at 500 × g for 10 minutes, and mononuclear cells enriched using a Histopaque-1077 density gradient. Red blood cells (RBCs) were lysed with ammonium chloride lysis [43]. Lung-derived cells from medial and diaphragmatic lobes were digested with collagenase (0.7 mg/ml) and DNase (0.03 mg/ml), filtered, and RBCs lysed before resuspension in DMEM containing 10% FBS, 1% PS, and 1% L-glutamine. All cells were cryopreserved in FBS with 10% DMSO and stored in liquid nitrogen until use.

Plaque assays

Viral load in nasal swabs was measured by plaque assay using MDCK cells. Samples were serially diluted in DMEM with 0.1% BSA and inoculated onto confluent MDCK monolayers. After 1 hour at 37°C with 5% CO_2, the inoculum was removed, cells were washed with Dulbecco's Phosphate-Buffered Saline (DPBS), and an overlay medium containing DMEM, 0.3% BSA, 2.86 mM L-glutamine, 0.3% sodium bicarbonate, 14 mM HEPES, 0.007% dextran, 1× PS, and 0.6% agar (Oxoid) was added. Plates were incubated for 72 h at 37°C with 5% CO_2. Plaques for EAavH1N1 were visualized using 0.1% crystal violet [39]. For IDV, plaques were detected by immunoperoxidase staining due to the lack of distinct cytopathic plaques [16]. Briefly, cells were fixed with 500 μl of 30% formalin (F8775, Sigma–Aldrich) in PBS at 4°C overnight, washed, and permeabilized with 0.1% Triton X-100 (T9284, Sigma–Aldrich) in PBS for 15 minutes at room temperature. After blocking with SuperBlock™ Blocking Buffer (37515, Thermo Fisher Scientific), cells were incubated with cattle anti-IDV immune serum (kindly provided by Dr. Mariette Ducatez, University of Toulouse, France) for 60 minutes, washed, and then incubated with HRP-conjugated goat anti-cattle IgG-Fc (A100-104P, Bethyl Laboratories, Inc.) for 60 minutes. Plaques were visualized using 3-amino-9-ethylcarbazole (AEC) chromogenic substrate (AEC101, Sigma-Aldrich) according to the manufacturer's instructions. Viral titre were calculated as $\log_{10}$ *PFU*/ml by averaging plaque counts and adjusting for dilution.

RNA isolation and quantification of viral genomic RNA

Genomic RNA (gRNA) copies of IDV-NP and EAavH1N1-M1 were quantified in NS by qRT-PCR [43]. Viral RNA was extracted from 200 μl of each sample and from purified virus stocks using the QIAamp Viral RNA Mini Kit (52906, Qiagen) according to the manufacturer's instructions. Standards were generated by isolating gRNA from purified IDV and EAavH1N1 viruses. Copy numbers per μl were calculated, and 10-fold serial dilutions from 1×10^{10} to 10 copies were prepared. Standard dilutions were included on each qRT-PCR plate with test samples. Reverse transcription and amplification were performed using the EXPRESS One-Step Superscript™ qRT-PCR Kit (11781200, Invitrogen) on an AriaMx Real-time PCR System (Agilent), following the thermal cycling conditions in Supplementary Table S6. Custom gene expression assays were designed using sequences from GenBank, NCBI (accession numbers OP474075.1, OP458677.1, MW362720.1, OP458613.1, OP458637.1, OP458685.1, MW362640.1). Primer and probe sequences are listed in Supplementary Table S6. Each sample and standard was run in duplicate. Standard curves were generated for each plate, and PCR efficiency (E) was calculated from the slope of the regression line using $E = 10(-1/\text{slope})$. Viral RNA copy numbers in experimental samples were determined by extrapolating cycle threshold (Ct) values against the standard curve and expressed as $\log_{10}$ NP or M1 gRNA copies per mL of sample. No-template controls (NTCs) were included on each plate. All experiments were conducted in compliance with MIQE (Minimum Information for Publication of Quantitative Real-Time PCR Experiments) guidelines [44, 45].

Enzyme-linked immunosorbent assays (ELISA)

Endpoint ELISAs were used to quantify IDV- and EAavH1N1-specific IgG and IgA antibodies in serum, BAL, and nasal swabs, as

previously described [31, 35, 46]. Serum was collected on days 1, 5, 7, and 12 DPI. BAL was collected on days 1, 5, and 12 DPI; and NS was collected on days 1, 5, 7, and 10 DPI. Ninety-six–well plates were coated overnight at 4°C with IDV or EAavH1N1 virus in 0.05 M carbonate—bicarbonate buffer (pH 9.6) (Sigma-Aldrich). Plates were washed with DPBS containing 0.05% Tween-20 (Sigma-Aldrich) and blocked with 4% skimmed milk in PBS w/ 0.05% Tween-20 for 2 hours at room temperature. Two-fold serial dilutions of heat-inactivated serum (starting at 1:20), BAL (1:2), or nasal swabs (1:8) were prepared in blocking buffer and incubated in duplicate (1 hour at room temperature for serum and BALF; 16 hours for nasal swabs). Negative controls were included on each plate. After washing, plates were incubated with mouse anti-pig IgG-HRP (1:20 000) or anti-pig IgA-HRP (1:10 000) (A100-102P, Bethyl Laboratories, Inc.) in blocking buffer for one hour at room temperature, washed, and developed with TMB substrate (50 µl/well) (34029, Thermo Scientific). Reactions were stopped with 1 M H_2SO_4 (50 µl/well), and absorbance was measured at 450 nm with a 630 nm reference using a VersaMax microplate reader (Molecular Devices). Endpoint titres were defined as the $\log_{10}$ of the highest dilution exceeding the cut-off (mean plus three standard deviations of negative controls or control animals).

Microneutralization assay

Neutralizing antibody (nAb) titres in serum and BAL were measured using a microneutralization (MN) assay as previously described [43, 45, 47]. Samples were heat-inactivated at 56°C for 30 minutes, serially diluted two-fold in virus growth medium (VGM; DMEM with 0.2% BSA, 1× PS, and 2 µg/ml TPCK-trypsin), and combined with live IDV or EAavH1N1 viruses. The initial dilution was 1:20 for serum and 1:2 for BAL. Viruses were diluted to 1:50 (IDV) or 1:200 (EAavH1N1) in VGM. Control wells included medium only (negative) and virus + cells only (positive). After a 2-hour incubation at 37°C with 5% CO_2, 3×10^4 MDCK cells per well were added to VGM, and plates were incubated overnight under the same conditions. Following incubation, cells were fixed with cold 4% paraformaldehyde (J61984.AP, Thermo Scientific) for 15 minutes, permeabilized with DPBS containing 0.05% Triton X-100 and 0.75 M glycine (50046, Sigma-Aldrich) for 30 minutes at room temperature, and washed with DPBS-T. Plates were incubated with primary antibodies [anti-influenza A NP (1:3500) (MCA2751, Bio-Rad) and cattle anti-IDV serum (1:200)] in SuperBlock™ buffer, followed by HRP-conjugated anti-mouse IgG (1:3500) (STAR207P, Bio-Rad) or anti-cattle IgG (MCA2439P, Bio-Rad) (1:1000) in SuperBlock™ buffer for 1 hour at room temperature. After washing, plates were developed with TMB substrate (50 µl per well), and reactions were stopped with 1 M H_2SO_4 (50 µl per well). Absorbance was measured at 450 nm with a 630 nm reference using a VersaMax microplate reader (Molecular Devices). MN titres were defined as the log10 50% inhibitory dilution ($\log10ID_{50}$), calculated as the dilution corresponding to the midpoint between the optical densities of virus-infected (positive control) and uninfected (negative control) wells, determined by linear interpolation from the titration curve.

Enzyme-linked immunospot (ELISpot)

Cryopreserved cells from BAL, TBLN, spleen, and PBMC were used to assess IFNγ- and IL-2-producing cell frequencies by ELISpot, as previously described [31, 46]. Multiscreen® 96-well plates (MCE membrane, MAHAS4510; Merck Millipore) were coated overnight at 4°C with either 1 µg/ml anti-pig IFNγ (clone P2G10; BD Pharmingen) in carbonate–bicarbonate (CBC) buffer or 10 µg/ml anti-pig IL-2 (clones MT264/267; Mabtech) in DPBS. Plates were washed with PBS and blocked with complete culture medium (RPMI 1640 with 10% FBS, 1X PS) for 2 hour at 37°C. Cells (2.5×10^5/well) were seeded in triplicate and stimulated with live IDV or EAavH1N1 (MOI = 1), Concanavalin A as a positive control (00-4978-03, Invitrogen), or culture medium as a negative control. After 48 hours incubation at 37°C with 5% CO_2, plates were washed with PBS-T and incubated for one hour at room temperature with biotinylated anti-pig IFN-γ (0.5 µg/ml; clone P2C11, BD Pharmingen) or anti-pig IL-2 (0.5 µg/ml; clone MT265, Mabtech). Plates were washed and incubated with streptavidin–alkaline phosphatase (1:1000; S291, Invitrogen) for 1 hour at room temperature, then developed with BCIP/NBT substrate (1706432, Bio-Rad) according to the manufacturer's instructions. Reactions were stopped after 20 min with tap water, and plates were air-dried. Spots were counted using the CTL ImmunoSpot® M6 automated analyser (CTL, Cleveland, OH, USA) and analysed with ImmunoSpot® Software version 7.1. Results were presented as the number of IFNγ- or IL-2-producing cells per 10^6 stimulated cells, after subtracting background spots from medium controls.

Intracellular cytokine staining (ICS)

IDV and EAavH1N1-specific $CD4^+$, $CD8^+$, and γδ T-cell responses were quantified by ICS assays using cells isolated from BAL, TBLN, PBMC, spleen, and MLN as previously described [31, 46]. For each tissue, 2×10^6 cells were resuspended in 200 µl RPMI with 10% FBS and 1× PS, then exposed to one of three conditions: (i) mock unstimulated, (ii) virus-stimulated (MOI = 1), or (iii) PMA + ionomycin (1×; 00497593, Invitrogen) as a positive control. Virus-stimulated and mock cultures were incubated at 37°C for 16 h, while PMA + ionomycin cultures were incubated for four hours in a CO_2 incubator. GolgiPlug (555029, BD Biosciences) was added 4 hours before staining. After stimulation, cells were washed in DPBS or BD Perm/Wash buffer (555028, BD Biosciences) as appropriate. All staining steps were performed in 50 µl with pre-titrated antibodies. Cells were harvested (520×g, 5 min, 4°C), washed twice in DPBS, and stained with mouse anti-γδ TCR for 20 min at 4°C. Following another wash, cells were incubated with anti-mouse IgG–BUV395 for 20 min at 4°C in the dark, then blocked with anti-mouse serum and washed twice with DPBS. Surface staining was performed with LIVE/DEAD™ Fixable Near-IR (Invitrogen), CD3, CD4α, and CD8β for 20 min at 4°C in the dark. After two additional DPBS washes, cells were fixed and permeabilized with BD CytoFix/CytoPerm for 15 min at 4°C. Intracellular staining for IFN-γ and TNF was conducted in 1× Perm/Wash buffer for 30 min at 4°C in the dark. Cells were washed twice, resuspended in 200 µl 1× Perm/Wash buffer. Further details of antibodies used are listed in Supplementary Table S6. Samples were acquired on a Cytek Aurora spectral flow cytometer, unmixed by SpectroFlo software (Cytek) using single-stained controls, and analysed in FlowJo v10 (BD Biosciences).

Single cell RNA-Seq library preparation and sequencing

Single-cell suspensions were prepared from lung tissues of 20 pigs for transcriptomic profiling using the 10× Genomics 3′ Gene Expression platform. Suspensions were adjusted to 10 000 cells per sample and encapsulated with the Chromium iX Controller, Next GEM Chip G, and the Single Cell 3′ v3.1 library preparation kit (10× Genomics, Pleasanton, CA, USA). Library quality and concentration were evaluated using the Qubit DNA Broad Range assay (Life Technologies, UK), Illumina Library Quantification Kit (New England Biolabs, USA), and TapeStation D5000 DNA assay (Agilent Technologies, USA). Libraries were pooled and sequenced on two NextSeq 2000 P4 100-cycle runs (Illumina, San Diego, CA, USA), each with a 1% PhiX control, targeting approximately 200 million reads per sample. Sequencing was performed according to the manufacturer's recommendations.

Single-cell RNA-seq data pre-processing and quality control

Single-cell RNA-seq profiles from 20 samples were analysed. Raw BCL files were demultiplexed using the mkfastq pipeline in Cell Ranger v7.1.0 (10× Genomics). Reads were aligned to the Sus scrofa reference genome (assembly 11.1; GCA_000003025.6) using STAR v2.7.2a within Cell Ranger, and UMI counts were generated with the Cell Ranger count function. All downstream analyses were conducted in R v4.3.2. Stringent filtering was applied to ensure data quality and minimize technical artefacts. Empty and barcode-swapped droplets were removed using DropletUtils v1.22.0 [48, 49]. Cells with total UMI counts above 50 000 or below 1000 were excluded to remove potential multiplets and low-quality cells. Additional filtering excluded cells with fewer than 500 detected genes, high mitochondrial gene content (>20%), or those predicted as doublets by scds v1.18.0. Genes with zero expression across all cells were also excluded. Library size differences were corrected using scaling normalization with computePooledFactors from the scuttle package v1.12.0, followed by log2 transformation with a pseudo-count of 1 [50]. Fourteen samples from three independent sequencing runs were integrated using the fastMNN algorithm in the batchelor package v1.18.1 to correct for batch effects [51].

Clustering and annotation of scRNA-seq libraries

Shared nearest-neighbour (SNN) graph-based clustering was performed using the clusterCells function in bluster v1.12.0. The top 5000 highly variable genes were identified with getTopHVGs from the scran package v1.30.2 [52]. Clustering was based on a Jaccard-weighted graph and the Louvain community detection algorithm, with k set to 25 nearest neighbours. This process identified 37 transcriptionally distinct clusters. Clusters were annotated using canonical marker genes and grouped into three main cell compartments: myeloid, lymphoid (T, B, and NK-like T cells), and non-immune structural cells. Differences in immune cell composition between groups were assessed using permutational multivariate analysis of variance (PERMANOVA) in the vegan package v2.7-2. Prior to analysis, cell proportion data were transformed using centred log-ratio (CLR) scaling with the compositions package v2.0-9. Data visualization and statistical summaries were generated using dplyr v1.1.4, tidyr v1.3.1, ggplot2 v3.4.3, and rstatix v0.7.3. Within each subset, cells were re-integrated and re-clustered using the same analytical framework to improve resolution. In the myeloid subset, 18 refined clusters were identified and annotated. Clusters 21 and 22, considered probable contaminants, were excluded from the final UMAP visualization. In the lymphoid subset, 19 clusters were identified, representing activated, cytotoxic, memory, and unconventional T-cell populations. In the non-immune structural compartment, 20 clusters were resolved. Cluster 13, identified as immune cell-derived noise, was removed from the final UMAP representation because it did not correspond to structural cell types. Across all subsets, clusters were manually annotated using conventional cell-type nomenclature based on marker gene expression (Supplementary Table S6). For each cluster, the most informative differentially expressed genes were identified using the scoreMarkers function in scran v1.30.2 to define cluster-specific transcriptional signatures.

Cell type scRNA-seq differential abundance and expression analyses

Differential abundance (DA) of cell subpopulations was evaluated across three major cell compartments under each experimental condition (control, EAavH1N1-, and IDV-infection) at 1 and 12 DPI. DA testing used edgeR v4.6.3 in R, applying a negative binomial generalized linear model (GLM) with empirical Bayes quasi-likelihood F-tests. The model included experimental condition as the main factor and sequencing run as a covariate to address batch effects. Sequencing depth was adjusted by including an offset based on cluster-level cell counts scaled to the total number of cells per sample. To prevent overfitting in clusters with limited replication, trend estimation was disabled during dispersion and quasi-likelihood dispersion estimation. Multiple testing was corrected using the Benjamini–Hochberg method. Pairwise DA comparisons included: at 1 DPI, IDV-infected ($n=3$) vs control ($n=3$); at 12 DPI, IDV-infected ($n=4$) vs control ($n=3$), EAavH1N1-infected ($n=4$) vs control ($n=3$), and IDV-infected ($n=4$) vs EAavH1N1-infected ($n=4$). Temporal changes within the IDV group were assessed by comparing samples at 1 DPI ($n=3$) and 12 DPI ($n=4$). Differential expression (DE) within each cell cluster was analysed using a pseudo-bulk approach, aggregating raw counts from all constituent cells to generate cluster-level profiles. Cluster–sample combinations with fewer than ten cells were excluded. Negative binomial GLMs were fitted for each cluster, and DE between experimental groups was assessed using empirical Bayes quasi-likelihood *F*-tests in edgeR v4.6.3, with sequencing run as a covariate. Multiple testing correction used the Benjamini–Hochberg procedure. Complete DE results are summarized in Supplementary Tables S1, S2, and S3.

Gene function and pathway enrichment scRNA-seq analysis

Adjusted *P*-values and $\log_2$ fold-change estimates from edgeR analyses were used for downstream functional and pathway

enrichment analyses with clusterProfiler v4.15.1. Gene set enrichment analysis (GSEA) was performed using KEGG pathway annotations [53, 54], applying a permutation-based approach to ranked gene lists ordered by $\log_2$ fold change to identify pathways with coordinated transcriptional changes. Resulting *P*-values were corrected for multiple testing using the Benjamini–Hochberg method. Significantly enriched KEGG pathways ($q < 0.05$) were visualized using bubble plots. Complete GSEA results are provided in Supplementary Tables S4 and S5.

Statistical analysis

Statistical analyses were performed using GraphPad Prism v10.5.0 (GraphPad Software, San Diego, CA, USA). Data normality was assessed prior to analysis. Parametric data were evaluated with unpaired *t*-tests, one-way ANOVA, or two-way ANOVA, followed by Tukey's or Dunnett's *post hoc* tests. Non-parametric data were analyzed using the Kruskal–Wallis test with Dunn's multiple comparisons test. Statistical significance was set at ($*P < 0.05$, $**P < 0.01$, $***P < 0.001$, $****P < 0.0001$), and the specific test used is indicated in the figure legends.

Acknowledgements

We thank the animal staff at The Pirbright Institute for their exemplary animal care and authors would also like to acknowledge the Pirbright Flow Cytometry facility, Sequencing and Bioinformatics Science Technology Platform, and support through the Core Capability Grant (BBS/E/PI/23NB0003). We thank Dr. Mariette Ducatez from the University of Toulouse, France, for providing the anti-IDV cattle serum. The Editor-in-Chief, Simon Milling, and handling editor, Emily Gwyer Findlay, would like to thank reviewers Mick Bailey and Anne Moore, for their contribution to the publication of this article.

Author contributions

Ashutosh Vats (Data curation, Formal analysis, Investigation, Methodology, Software, Supervision, Validation, Visualization, Writing—original draft, Writing—review & editing), Liu Yang (Data curation, Formal analysis, Investigation, Methodology, Software, Validation, Visualization, Writing—review & editing), Ehsan Sedaghat-Rostami (Investigation, Methodology, Visualization, Writing—review & editing), Catherine Hatton (Methodology, Writing—review & editing), Emily Briggs (Methodology, Writing—review & editing), Graham Freimanis (Data curation, Investigation, Methodology, Writing—review & editing), Tim Downing (Data curation, Investigation, Methodology), Kristein Van Reeth (Funding acquisition, Investigation, Methodology, Resources, Writing—review & editing), Basudev Paudyal (Methodology, Supervision, Writing—review & editing), Francisco J. Salguero (Data curation, Formal analysis, Investigation, Methodology, Software, Validation, Visualization, Writing—review & editing), Wilhelm Gerner (Conceptualization, Formal analysis, Investigation, Methodology, Supervision, Validation, Visualization, Writing—original draft, Writing—review & editing), and Elma Tchilian (Conceptualization, Formal analysis, Funding acquisition, Investigation, Methodology, Project administration, Resources, Supervision, Visualization, Writing—original draft, Writing—review & editing)

Supplementary material

Supplementary material is available at *Discovery Immunology* online.

Conflicts of interest

All authors declare no conflict of interests.

Funding

This research was supported by the UKRI Biotechnology and Biological Sciences Research Council (BBSRC) IAA award BB/X019780/1 as part of the EPICVIR project at the International Collaboration of Research on Infectious Animal Diseases (ICRAD). Research at Pirbright received funding from BBSRC through the Pirbright Institute's Strategic Programme Grants (ISPGs) [BBS/E/PI/230002A; BBS/E/PI/230002B and BBS/E/PI/230002C], as well as the BBSRC National Bioscience Research Infrastructure: High Containment and Low Containment Services and Science Platforms grants [BBS/E/PI/23NB0004, BBS/E/PI/23NB0003].

Data and code availability

All R scripts used for processing and analysis of the scRNA-seq data are available at: https://github.com/LynnGoodnight/bsp306. Fastq and h5 files from sequencing are available at GEO under accession number GSE331071: https://www.ncbi.nlm.nih.gov/geo/query/acc.cgi?acc=GSE331071.

Ethical approval

All experiments were approved by the Pirbright Institute Ethical Review Committee and conducted in accordance with the U.K. Government Animal (Scientific Procedures) Act 1986 under Project License PP2064443. The Pirbright Institute conforms to ARRIVE guidelines (https://arriveguidelines.org/arrive-guidelines).

Permission to reproduce

Not applicable

Clinical trial registration

Not applicable

Data Availability

All data generated or analyzed that are critical to the reported findings are available within the article and its Supplementary material files. Additional supporting data are available from the corresponding authors without undue reservation.

References

1. Iuliano AD, Roguski KM, Chang HH, Muscatello DJ, Palekar R, Tempia S, *et al.* Estimates of global seasonal influenza-associated respiratory mortality: a modelling study. *Lancet* 2018, **391**, 1285–300.
2. Vandegrift KJ, Sokolow SH, Daszak P, Kilpatrick AM. Ecology of avian influenza viruses in a changing world. *Ann N Y Acad Sci* 2010, **1195**, 113–28.
3. Ma W, Kahn RE, Richt JA. The pig as a mixing vessel for influenza viruses: human and veterinary implications. *J Mol Genet Med* 2008, **3**, 158–66.
4. Smith GJD, Vijaykrishna D, Bahl J, Lycett SJ, Worobey M, Pybus OG, *et al.* Origins and evolutionary genomics of the 2009 swine-origin H1N1 influenza A epidemic. *Nature* 2009, **459**, 1122–5.
5. He Y, Song S, Wu J, Wu J, Zhang L, Sun L, *et al.* Emergence of Eurasian avian-like swine influenza A (H1N1) virus in a child in Shandong Province, China. *BMC Infect Dis* 2024, **24**, 550.
6. Parys A, Vereecke N, Vandoorn E, Theuns S, Van Reeth K. Surveillance and genomic characterization of influenza A and D viruses in swine, Belgium and the Netherlands, 2019–2021. *Emerg Infect Dis* 2023, **29**, 1459–64.
7. Sun H, Xiao Y, Liu J, Wang D, Li F, Wang C, *et al.* Prevalent Eurasian avian-like H1N1 swine influenza virus with 2009 pandemic viral genes facilitating human infection. *Proc Natl Acad Sci U S A* 2020, **117**, 17204–10.
8. Zou J, Jiang M, Xiao R, Sun H, Liu H, Peacock T, *et al.* GGCX promotes Eurasian avian-like H1N1 swine influenza virus adaption to interspecies receptor binding. *Nat Commun* 2025, **16**, 670.
9. Meng F, Yang H, Qu Z, Chen Y, Zhang Y, Zhang Y, *et al.* A Eurasian avian-like H1N1 swine influenza reassortant virus became pathogenic and highly transmissible due to mutations in its PA gene. *Proc Natl Acad Sci U S A* 2022, **119**, e2203919119.
10. Eggink D, Kroneman A, Dingemans J, Goderski G, van den Brink S, Bagheri M, *et al.* Human infections with Eurasian avian-like swine influenza virus detected by coincidence via routine respiratory surveillance systems, the Netherlands, 2020 to 2023. *Euro Surveill* 2025, **30**, 2400662.
11. van der Vries E, Germeraad EA, Kroneman A, Dieste-Pérez L, Eggink D, Willems E, *et al.* Swine influenza virus surveillance programme pilot to assess the risk for animal and public health, the Netherlands, 2022 to 2023. *Euro Surveill* 2025, **30**, 2400664.
12. Sun H, Liu J, Xiao Y, Duan Y, Yang J, Chen Y, *et al.* Pathogenicity of novel reassortant Eurasian avian-like H1N1 influenza virus in pigs. *Virology* 2021, **561**, 28–35.
13. Lan R, Yang J, Li J, Li H, Cao X, Tao M, *et al.* Continuous evolution of Eurasian avian-like H1N1 swine influenza viruses with pdm/09-derived internal genes enhances pathogenicity in mice. *J Virol* 2025, **99**, e0043025.
14. Limaye S, Lohar T, Dube H, Ramasamy S, Kale M, Kulkarni-Kale U, *et al.* Rapid evolution leads to extensive genetic diversification of cattle flu influenza D virus. *Commun Biol* 2024, **7**, 1276.
15. Su S, Fu X, Li G, Kerlin F, Veit M. Novel influenza D virus: epidemiology, pathology, evolution and biological characteristics. *Virulence* 2017, **8**, 1580–91.
16. Ishida H, Murakami S, Kamiki H, Matsugo H, Katayama M, Sekine W, *et al.* Construction of an influenza D virus with an eight-segmented genome. *Viruses* 2021, **13**, 2166.
17. Song H, Qi J, Khedri Z, Diaz S, Yu H, Chen X, *et al.* An open receptor-binding cavity of hemagglutinin-esterase-fusion glycoprotein from newly-identified influenza D virus: basis for its broad cell tropism. *PLoS Pathog* 2016, **12**, e1005411.
18. Uprety T, Sreenivasan CC, Yu J, Zhao M, Liu R, Yu H, *et al.* Differential tissue tropism and transmission efficiency of two dominant influenza D clades with overlapping but distinct receptor binding fine specificities in ferrets. *PLoS Pathog* 2025, **21**, e1013493.
19. Hause BM, Collin EA, Liu R, Huang B, Sheng Z, Lu W, *et al.* Characterization of a novel influenza virus in cattle and swine: proposal for a new genus in the orthomyxoviridae family. *mBio* 2014, **5**, e00031–14.
20. Chiapponi C, Faccini S, De Mattia A, Baioni L, Barbieri I, Rosignoli C, *et al.* Detection of influenza D virus among swine and cattle, Italy. *Emerg Infect Dis* 2016, **22**, 352–4.
21. Ferguson L, Luo K, Olivier AK, Cunningham FL, Blackmon S, Hanson-Dorr K, *et al.* Influenza D virus infection in feral swine populations, United States. *Emerg Infect Dis* 2018, **24**, 1020–8.
22. White SK, Ma W, McDaniel CJ, Gray GC, Lednicky JA. Serologic evidence of exposure to influenza D virus among persons with occupational contact with cattle. *J Clin Virol* 2016, **81**, 31–3.
23. Trombetta CM, Montomoli E, Di Bartolo I, Ostanello F, Chiapponi C, Marchi S. Detection of antibodies against influenza D virus in swine veterinarians in Italy in 2004. *J Med Virol* 2022, **94**, 2855–9.
24. Leibler JH, Abdelgadir A, Seidel J, White RF, Johnson WE, Reynolds SJ, *et al.* Influenza D virus exposure among US cattle workers: a call for surveillance. *Zoonoses Public Health* 2023, **70**, 166–70.
25. Vega-Rodriguez W, Ly H. Epidemiological, serological, and genetic evidence of influenza D virus infection in humans: is it a justifiable cause for concern? *Virulence* 2023, **14**, 2150443.
26. Sanders CG, Liu M, Fusco JA, Ohl EM, Tarbuck NN, King EM, *et al.* Efficient replication of influenza D virus in the human airway underscores zoonotic potential. *Proc Natl Acad Sci U S A* 2026, **123**, e2530325123.
27. Salem E, Hägglund S, Cassard H, Corre T, Näslund K, Foret C, *et al.* Pathogenesis, host innate immune response, and aerosol transmission of influenza D virus in cattle. *J Virol* 2019, **93**, e01853-18.
28. Lion A, Secula A, Rançon C, Boulesteix O, Pinard A, Deslis A, *et al.* Enhanced pathogenesis caused by influenza D virus and *Mycoplasma bovis* coinfection in calves: a disease severity linked with overexpression of IFN-γ as a key player of the enhanced innate immune response in lungs. *Microbiol Spectr* 2021, **9**, e0169021.
29. Liu R, Sheng Z, Huang C, Wang D, Li F. Influenza D virus. *Curr Opin Virol* 2020, **44**, 154–61.
30. Kaplan BS, Falkenberg S, Dassanayake R, Neill J, Velayudhan B, Li F, *et al.* Virus strain influenced the interspecies transmission of influenza D virus between calves and pigs. *Transbound Emerg Dis* 2021, **68**, 3396–404.
31. Vatzia E, Allen ER, Manjegowda T, Morris S, McNee A, Martini V, *et al.* Respiratory and intramuscular immunization with

ChAdOx2-NPM1-NA induces distinct immune responses in H1N1pdm09 Pre-exposed pigs. *Front Immunol* 2021, **12**, 763912.
32. Duerrwald R, Schlegel M, Bauer K, Vissiennon T, Wutzler P, Schmidtke M. Efficacy of influenza vaccination and tamiflu® treatment—comparative studies with eurasian swine influenza viruses in pigs. *PLoS One* 2013, **8**, e61597.
33. De Vleeschauwer AR, Van Poucke SG, Karasin AI, Olsen CW, Van Reeth K. Cross-protection between antigenically distinct H1N1 swine influenza viruses from Europe and North America. *Influenza Other Respir Viruses* 2011, **5**, 115–22.
34. Zhu W, Feng Z, Chen Y, Yang L, Liu J, Li X, *et al.* Mammalian-adaptive mutation NP-Q357K in Eurasian H1N1 swine influenza viruses determines the virulence phenotype in mice. *Emerg Microbes Infect* 2019, **8**, 989–99.
35. Yang H, Chen Y, Qiao C, He X, Zhou H, Sun Y, *et al.* Prevalence, genetics, and transmissibility in ferrets of Eurasian avian-like H1N1 swine influenza viruses. *Proc Natl Acad Sci U S A* 2016, **113**, 392–7.
36. Gao H, Sun W, Lu P, Dong Z, Wu J, Li Y, *et al.* Efficient airborne transmission of influenza D virus in ferret models and serological evidence of human exposure in Northeast China. *Emerg Microbes Infect* 2025, **14**, 2564308.
37. Sreenivasan C, Thomas M, Sheng Z, Hause BM, Collin EA, Knudsen DEB, *et al.* Replication and transmission of the novel bovine influenza D virus in a Guinea pig model. *J Virol* 2015, **89**, 11990–2001.
38. Chen Z, Zeng Y, Wei Y, Wang Q, Liu M, Zhang B, *et al.* Influenza D virus matrix protein 1 restricts the type I interferon response by degrading TRAF6. *Virology* 2022, **568**, 1–11.
39. Morgan SB, Hemmink JD, Porter E, Harley R, Shelton H, Aramouni M, *et al.* Aerosol delivery of a candidate universal influenza vaccine reduces viral load in pigs challenged with pandemic H1N1 virus. *J Immunol* 2016, **196**, 5014–23.
40. Holzer B, Morgan SB, Matsuoka Y, Edmans M, Salguero FJ, Everett H, *et al.* Comparison of heterosubtypic protection in ferrets and pigs induced by a single-cycle influenza vaccine. *J Immunol* 2018, **200**, 4068–77.
41. Gauger PC, Vincent AL, Loving CL, Henningson JN, Lager KM, Janke BH, *et al.* Kinetics of lung lesion development and pro-inflammatory cytokine response in pigs with vaccine-associated enhanced respiratory disease induced by challenge with pandemic (2009) A/H1N1 influenza virus. *Vet Pathol* 2012, **49**, 900–12.
42. Chrun T, Maze EA, Vatzia E, Martini V, Paudyal B, Edmans MD, *et al.* Simultaneous infection with porcine reproductive and respiratory syndrome and influenza viruses abrogates clinical protection induced by live attenuated porcine reproductive and respiratory syndrome vaccination. *Front Immunol* 2021, **12**, 758368.
43. McNee A, Smith TRF, Holzer B, Clark B, Bessell E, Guibinga G, *et al.* Establishment of a pig influenza challenge model for evaluation of monoclonal antibody delivery platforms. *J Immunol* 2020, **205**, 648–60.
44. Bustin SA, Benes V, Garson JA, Hellemans J, Huggett J, Kubista M, *et al.* The MIQE guidelines: minimum information for publication of quantitative real-time PCR experiments. *Clin Chem* 2009, **55**, 611–22.
45. Faccini S, De Mattia A, Chiapponi C, Barbieri I, Boniotti MB, Rosignoli C, *et al.* Development and evaluation of a new real-time RT-PCR assay for detection of proposed influenza D virus. *J Virol Methods* 2017, **243**, 31–4.
46. Edmans M, McNee A, Porter E, Vatzia E, Paudyal B, Martini V, *et al.* Magnitude and kinetics of T cell and antibody responses during H1N1pdm09 infection in inbred babraham pigs and outbred pigs. *Front Immunol* 2021, **11**, 604913.
47. Powell TJ, Silk JD, Sharps J, Fodor E, Townsend ARM. Pseudotyped influenza A virus as a vaccine for the induction of heterotypic immunity. *J Virol* 2012, **86**, 13397–406.
48. Griffiths JA, Richard AC, Bach K, Lun ATL, Marioni JC. Detection and removal of barcode swapping in single-cell RNA-seq data. *Nat Commun* 2018, **9**, 2667.
49. Lun ATL, Riesenfeld S, Andrews T, Dao TP, Gomes T, Marioni JC. EmptyDrops: distinguishing cells from empty droplets in droplet-based single-cell RNA sequencing data. *Genome Biol* 2019, **20**, 63.
50. McCarthy DJ, Campbell KR, Lun ATL, Wills QF. Scater: pre-processing, quality control, normalization and visualization of single-cell RNA-seq data in R. *Bioinformatics* 2017, **33**, 1179–86.
51. Haghverdi L, Lun ATL, Morgan MD, Marioni JC. Batch effects in single-cell RNA-Sequencing data are corrected by matching mutual nearest neighbors. *Nat Biotechnol* 2018, **36**, 421–7.
52. Lun AT, McCarthy DJ, Marioni JC. A step-by-step workflow for low-level analysis of single-cell RNA-seq data with bioconductor. *F1000Res* 2016, **5**, 2122.
53. Boyle EI, Weng S, Gollub J, Jin H, Botstein D, Cherry JM, *et al.* GO::TermFinder—open source software for accessing gene ontology information and finding significantly enriched gene ontology terms associated with a list of genes. *Bioinformatics* 2004, **20**, 3710–5.
54. Subramanian A, Tamayo P, Mootha VK, Mukherjee S, Ebert BL, Gillette MA, *et al.* Gene set enrichment analysis: a knowledge-based approach for interpreting genome-wide expression profiles. *Proc Natl Acad Sci U S A* 2005, **102**, 15545–50.